J Therm Anal Calorim (2010) 101:33–40
DOI 10.1007/s10973-010-0829-2

Phase equilibria in binary subsystems of urea–biuret–water system

T. S. Babkina · A. V. Kuznetsov

RCCT2009 Special Chapter

Abstract Joint results of the differential scanning calorimetry (DSC) and thermogravimetry (TG) experiments were the basis for the fusion enthalpy and temperature determination of the biuret $(NH_2CO)_2NH$ (synthesis by-product of the urea fertilizer $(NH_2)_2CO$). Recommended values are $\Delta_m H = (26.1 \pm 0.5)$ kJ mol^{-1}, $T_m = (473.8 \pm 0.4)$ K. The DSC method allowed for the phase diagrams of "water–biuret," "water–urea," "urea–biuret" binary systems to be studied; as a result, liquidus and solidus curves were precisely defined. Stoichiometry and decomposition temperature of the biuret hydrate identified, composition of the compound in "urea–biuret" system was suggested.

Keywords Urea · Biuret · Thermal decomposition · Enthalpy of fusion · Phase diagram · DSC · TG

Introduction

Urea ($(NH_2)_2CO$) is a high-demand fertilizer. Interaction of carbon dioxide and ammonia under both high pressure and temperature lies in the core of the industrial urea-making method. Biuret ($(NH_2CO)_2NH$) is a by-product, formed in the process of production stages of the "urea synthesis melt" distillation, which are accompanied by the rise of temperature. At 3% content, it negatively influences growth of plants. Conditions of producing carbamide with low biuret content can be predicted, requiring a modification of the "urea synthesis melt" model. A real object is comprised of many compounds: carbon dioxide, ammonia, water, urea, ammonium carbamate, ammonium carbonate, and other substances. Thermodynamic modeling of multicomponent systems traditionally proceeds from the lower dimension systems. Binary subsystems of the ternary "urea–biuret–water" system became the object of this study.

Sufficient information on thermodynamic properties of crystalline urea [1–10] and water [11] is available, but data on biuret are limited and contradictory. There is no common opinion regarding melting processes and biuret decomposition (both processes occur in the same temperature range). At 190–200 °C biuret melts and decomposes [12–17], though some authors adhere to the point of view that the process taking place is considered merely a decomposition. Melting temperature values cited by different authors vary from 179 to 195 °C. Seemingly, such divergences might occur as a result of the varying purity state of the reagent. In [13] biuret melting temperature of 193 °C and enthalpy of fusion of 28.8 kJ mol^{-1} were obtained, but no attempts to take into account the decomposition's contribution to the total DSC-measured effect were done. The objective of this study is to set apart contributions of the melting and chemical reactions to the process's total heat effect observed by DSC. The obtained data are necessary for phase equilibria calculation in every biuret-containing system.

There is one publication dealing with experimental construction of each binary system phase diagram of "urea–biuret" [18] and "water–biuret" [19].

Constructed in [19], the "urea–biuret" diagram represents a superposition of two diagrams: one with simple eutectic and another with the incongruently melting compound of 2:1. At high cooling rate the compound does not seem to form, and the

T. S. Babkina
Chemistry Department, Lomonosov Moscow State University, Leninskie Gory, Moscow 119991, Russia

A. V. Kuznetsov (✉)
Department of Materials Science, Lomonosov Moscow State University, Leninskie Gory, Moscow 119991, Russia
e-mail: alexander.kuzn@gmail.com

eutectic temperature is 106 °C. In case of slow cooling, a stable equilibrium takes place, eutectic is at 111 °C. While studying the aforementioned system, it is necessary to figure out which equilibria are stable and which are metastable, as well as to define the exact composition and conditions of the stoichiometric compound.

The incongruently melting biuret hydrate is formed in the "water–biuret" system. Coordinates of the peritectic point: 112.5 °C, 63.5 wt% $(NH_2CO)_2NH$. Spectral and structural properties of the biuret crystal hydrate were studied in the works [20–22]. In the 1898 year study (cited from [19]) it was noted that the hydrate composition might differ from that of 1:1. Information on the "water–biuret" system may be supplemented by identifying the composition and the stability region of the crystal hydrate. Considering that these binary systems have only one publication each, establishing the solidus and liquidus coordinates is required.

The "water–urea" system has been studied in quite a detail, there are verified data on solubility of the urea in water [23–27]. The part of the fusibility diagram of the "water–urea" system near the solvent angle is partially present in the studies [27, 28]. The eutectic points in the mentioned publications were measured at low temperatures.

This study's purpose was to define: (1) the value of biuret thermodynamic functions of fusion; (2) data on diagrams of the binary systems, and also to specify of the binary compound compositions. These data allow to construct the thermodynamic phase models of the ternary system $(NH_2)_2CO$–$(NH_2CO)_2NH$–H_2O. In perspective (if the system dimensions increase) conditions of producing carbamide with low biuret content can be predicted.

Experimental

Biuret

A sample of the commercial ("Viking") pure-grade (99%) biuret reagent underwent extra recrystallization from water and ethanol twice. The solvent was evaporated at 120 °C and pressure of 0.1 Torr using an oil pump. The purity grade was estimated by the change of the NMR spectra. Purified reagent was characterized by means of DSC and XRD methods and element CHN analysis. During the entire study period biuret was kept in an airtight vessel, regularly checked for any impurities. No changes were observed.

Urea

Commercial urea reagent ("Reahim") of analytical grade (99%) was recrystallized from water. Single phase was confirmed by XRD and DSC methods.

Biuret hydrate $(NH_2CO)_2NH{\cdot}0.7H_2O$

The sample of biuret hydrate was obtained by the following method: a biuret shot was dissolved in distilled water while heating up to 80 °C. When the dissolution process ended, it was registered visually by the absence of any visible reagent particles or turbidness. The solution was slowly cooled to room temperature, the settled precipitate was filtered using a Buchner funnel and air-dried to a constant mass. Compound was characterized by means of TG, DSC, XRD, and CHN methods.

Methods

^1H NMR and *^{13}C NMR* spectra were run on a *Bruker Avance 400 DPX* spectrometer at an operating frequency of 400 and 100 MHz, respectively.

X-ray powder diffraction data were obtained with a Guinier-type focusing camera ($2\theta = 3 \div 100°$, step 0.005°). Measurement results were transferred to a computer. Obtained spectra were compared with the Joint Committee on Powder Diffraction Standards Powder Diffraction File-2 (JCPDS PDF-2) databank. Possible residual impurity content is 1 wt%.

Elemental analysis was carried out on the *Carlo–Erba Elemental Analyzer Model 1106* with the method's error at 0.3%.

Thermal analysis of biuret was performed via the differential scanning calorimeter *NETZSCH DSC 204 F1* in 25–230 °C temperature range at heating rates varying from 1 to 30 K min^{-1}. The differential scanning calorimeter was calibrated for every heating rate by a set of standards with known transition temperatures and enthalpies. The experiments were carried out in the flow of dried argon (flow rate was 10 or 20 mL min^{-1}), cooling was executed using a manual system with liquid nitrogen. The sample mass was approximately 5 mg.

Mass change measurements were done on *NETZSCH TG 209 F1* in the 50–230 °C temperature range. The experiments were conducted in the 10 mL min^{-1} flow of dry air. The sample mass was about 10–15 mg.

Analysis of evolved gas during biuret decomposition was performed on *NETZSCH STA Jupiter 449C* coupled with the Fourier transform infrared (FTIR) spectrometer *Bruker Tensor 27*. Sorption spectra were registered at the 700–4,000 cm^{-1} region, where linear dependence for the IR intensity (for the *Globar*™ emitter) and detector's sensibility (MCT D315) versus the wavelength took place.

Phase diagram investigation for the binary systems "water–biuret," "urea–biuret," "water–urea" was done using the differential scanning calorimeter *NETZSCH DSC 204 F1*.

The sample preparation and registration conditions (heating rate) were optimized during the preliminary experiments. The equilibrium transition was confirmed for every system.

Results and discussion

Thermal properties of urea

According to the literature data, urea is stable up to the fusion temperature of 133.5 °C under the standard pressure. A data summary on urea temperature and enthalpy of fusion found in the literature combined with our own results are in Table 1.

A joint DSC and TG experiment proved that urea melts without decomposing (see Fig. 1). With the scanning rate at 10 K min^{-1}, no mass loss prior to the start of the melting process took place, unlike the observation in [14]. After the melting stops, the mass loss is insignificant, reaching 0.3% at a minor temperature interval (2–3 K). Therefore, it appears that there is a small temperature range where liquid urea may exist. An experiment to define the specific heat capacity of liquid urea in the given temperature interval is shown as possible.

Table 1 A data summary on urea melting temperature and enthalpy of fusion found in the literature combined with our own results

T_m/°C	$\Delta_m H$/kJ mol^{-1}	Source
132.7	14.52	[29]
–	13.47 ± 0.25	[30]
132.8	13.61	[31]
133.0	14.41	[32]
132.0	15.52	[33]
132.8	13.9	[3]
133.5	14.79 ± 0.16	[34]
133.0	14.5	[4]
133.0	14.1	[13]
134.8	15.03 ± 0.12	[7]
134.3	15.13	Present study

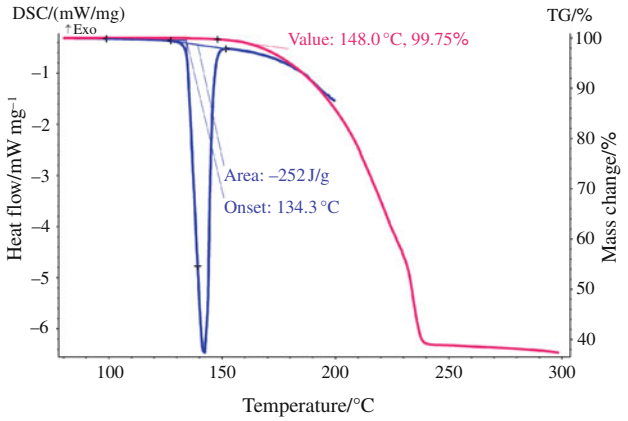

Fig. 1 The results of DSC and TG study of urea fusion process

Thermal properties of biuret

The experiments that were carried out with the heating rate of 10 K min^{-1} served the purpose of defining the thermodynamic melting functions of biuret. The DSC analysis and TG measurement were conducted simultaneously at the same heating rate. Obtained curves are presented in Fig. 2.

The endo-effect ($Q = 26.2$ kJ mol^{-1}) occurs at 198.0 °C, accompanied by mass loss (~6%). After the experiment, the biuret sample visually became agglutinate, covering the cell's walls like a film, but still being white. This proves the fact mentioned in the literature that heating of biuret causes simultaneous processes of fusion and chemical transformation. Biuret mass loss at fusion temperature is insignificant; nevertheless, such data cannot be used for further calculation. Attempts were done to estimate the contribution of the chemical decomposition reaction to the total value of the observed effect. Since the peak of the DSC curve (representing the decomposition process) is not clearly shown, the results of the DSC experiment could not be used directly to estimate the heat of the decomposition reaction. Thermogravimetry coupled with FTIR-analysis of evolved gas was performed in order to study in detail the progress of the pure biuret samples' decomposition at 190 °C.

According to the FTIR-spectra, residual quantities of CO_2 and H_2O are observed in the gas phase up to 170 °C. The amount of NH_3 increases gradually from 190 °C, and the CO_2 content in the gas also rises at 200–210 °C. It provides evidence of the biuret decomposition. The process may be described by the reactions like the ones presented in [15]:

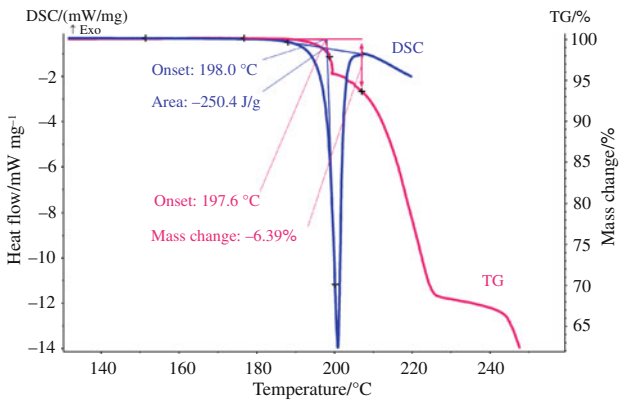

Fig. 2 The results of DSC and TG study of biuret thermolysis

$$2(NH_2CO)_2NH = 2NH_3\,(g) + HNCO\ (\text{cyanic acid},\ g) + C_3H_3N_3O_3(\text{cyanuric acid},\ s)$$

$$2(NH_2CO)_2NH = NH_3(g) + 2HNCO(\text{cyanic acid},\ g)$$

$$2(NH_2CO)_2NH = NH_2(OH)_2C_3N_3\,(\text{ammelide},\ s) + HNCO(\text{cyanic acid},\ g) + NH_3(g) + H_2O(g).$$

It is difficult to propose an exact decomposition mechanism since the obtained condensed products may be quite numerous. Gas phase composition results may be adequately described by each of the aforementioned processes.

We analyzed the heating rate influence on the observed effect in order to estimate the decomposition's contribution. DSC experiments were performed at heating rates varying from 1 to 20 K min^{-1}. The obtained data are presented in Fig. 3 and in Table 2.

Figure 3 shows that while heating rate steadily decreases with a reduction in effect temperature, the heat effect rises. (Due to different calibration conditions, the same square unit equals higher heat effect in case of lower scanning rate.) TG experiments at varying heating rates were conducted at the same time. We observed decreasing mass loss with increasing scanning rate.

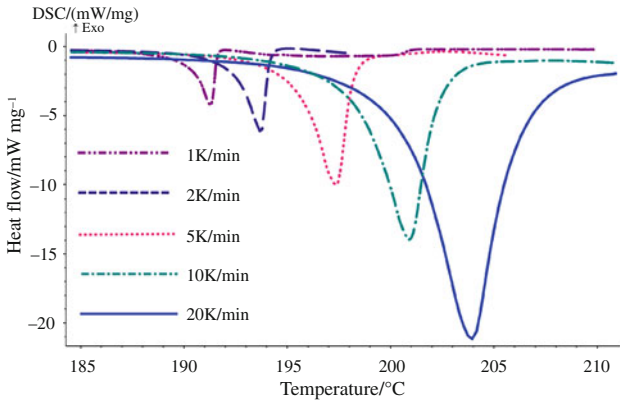

Fig. 3 The results of DSC study of biuret thermolysis using different scanning rates

Table 2 The onset temperature and specific heat of the biuret thermolysis, obtained at different heating rates by DSC

Heating rate/K min^{-1}	T_{onset}/°C	Q/J g^{-1}
1	190.3	299.7
2	192.3	278.0
5	195.4	271.0
10	198.2	253.4
20	200.3	253.4

To prove that the method's limitations did not cause the difference in effect value, we conducted a check experiment on a sample with tabulated enthalpy of fusion and melting temperature. Intermetallic InBi with the phase transition in the temperature range of our interest became our test subject. It was shown that in case of varying scanning rates, the relative error in the heat effect's value is at 2.3%. The distinction in heat effect values for biuret is significantly larger than that, reaching 8%.

Changing heating rates leads to a simultaneous decrease of the effect temperature and an increase of the heat effect. This temperature dependence can be described as similar to the cryoscopic effect. According to DSC and TG data, biuret phase decomposition precedes the melting process (Fig. 2). The resultant condensed product of the decomposition acts as an impurity and decreases the mixture's melting temperature. If the heating rate increases, higher temperatures are required to set off the decomposition process. At the same time, the amount of decomposition products decreases, which explains the difference between the effect temperature and the biuret melting temperature being reduced.

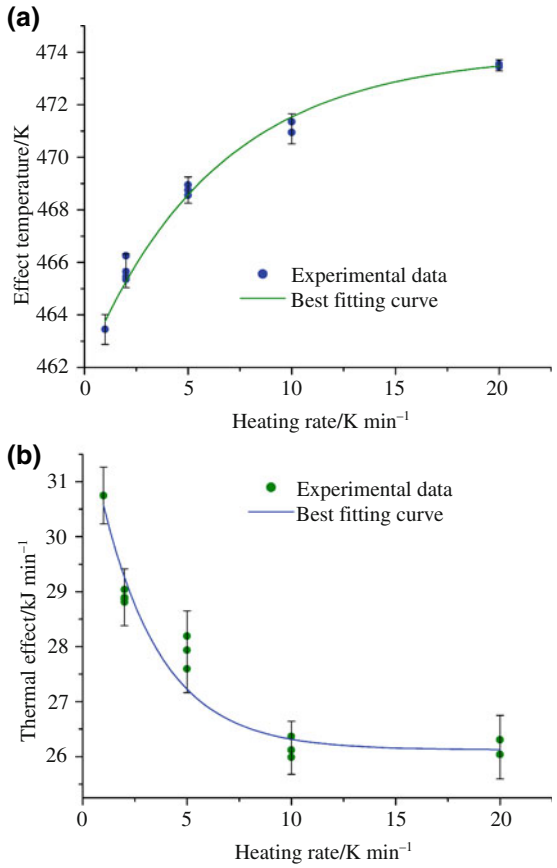

Fig. 4 Approximation of thermal effects and effect temperatures as a function of scanning rate using the correlation: $y = y_0 + A \cdot \exp(-v/t)$, where **a**: $y_0 = 473.8$, $A = -12.0$, $t = 6.3$; **b**: $y_0 = 26.1$, $A = 6.29$, $t = 2.9$

The figure shows the experimental values of effect heats and temperatures versus scanning rates: $T = f(v)$ (Fig. 4a), $Q = f(v)$ (Fig. 4b), where v equals heating rate. Approximation of the obtained data provided the basis for evaluating the biuret fusion properties. The estimation was based on the fact that a phase transition takes place at a fixed temperature, whereas a chemical reaction occurs at a temperature range (since the latter's effects on TG and DSC are defined by the process' kinetics, not thermodynamics). Altering the heating rate made the contribution of decomposition reaction to the total heat effect vary. Thus, in the limit of infinitely high scanning rates, the chemical reaction's contribution may be neglected. After the approximation of experimental data using the correlation ($y = y_0 + A \cdot \exp(-v/t)$), biuret melting temperature $T_m = (473.8 \pm 0.4)$ K and enthalpy of fusion $\Delta_m H = (253 \pm 4)$ J g^{-1}, or (26.1 ± 0.5) kJ mol^{-1} were estimated.

During the check experiment at 30 K min^{-1}, we observed the effect temperature of $T_{onset} = 473.5$ K. It agrees with the approximation.

Urea–biuret system

Special attention was given to the improvement of the region near the eutectic point. There were seven samples with biuret concentration varying from 1 to 46 mol% prepared.

DSC curve has one more peak corresponding to metastable eutectic at the heating rate of 5 K min^{-1}. The data are similar to the ones obtained in the study [18]. Most likely, the metastable eutectic can be observed due to slow kinetics of the binary compound synthesis. In 20 days, the sample of 6.2 mol% $(NH_2CO)_2NH$ was tested again in the same registration conditions (the sample had been kept in an airtight vessel). However, the DSC curve had changed; the first peak became hardly noticeable (Fig. 5). It was indicated that the same peak hadn't been registered at 1 K min^{-1}, either. System components probably could not fully react and generate a compound at high heating rates, that is why a metastable eutectic based on pure components is present.

Results of the experimental series are generalized in Table 3.

Figure 6 shows the results of this study (squares) and [18] (diamonds). The stoichiometric phase and solidus curves are depicted as lines. Our results confirm the conditions of the compound's peritectic decomposition and the position of the left liquidus curve. However, the solidus curve has higher temperatures compared to the data in [18]. The same goes for the metastable solidus line. In case of the sample with 46 mol% of biuret, special attention ought to be paid to the number of registered effects. If the binary compound appears to be 2:1, then we should have obtained two effects instead of the observed three. Our data act as

Table 3 Liquidus, solidus, metastable eutectic, and peritectic points for the "urea–biuret" system

Biuret mole concentration/%	t/°C (metastable)	t/°C (solidus)	t/°C (liquidus)	t/°C (peritectic)
1.1	108.5	112.9	133.9	
2.8	106.9	112.3	130.8	
6.2	107.8	113.0	127.2	
19.8	107.4	–	114.8	
22.9	107.9	112.9	114.6	
23.9		114.4	117.2	
31.8	107.4	112.2	–	116.6
46.1	107.7	113.0	–	116.7
66.2			170.0	

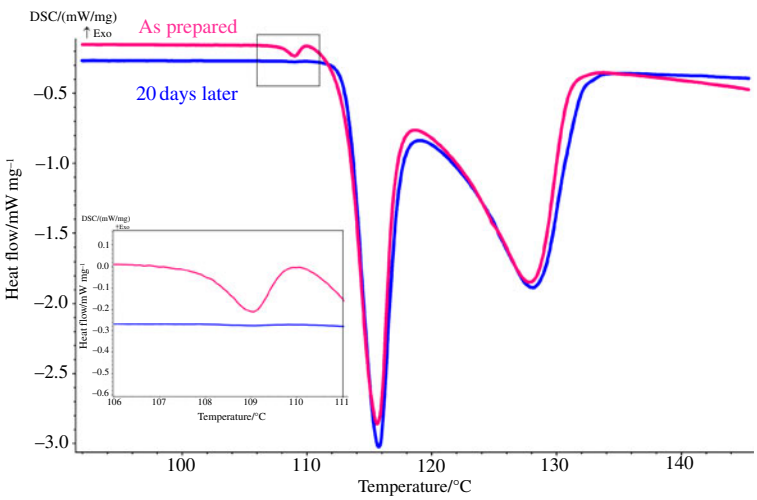

Fig. 5 DSC curves of the "urea–biuret" mixture (6.2 mol% biuret) as prepared and 20 days kept in airtight vessel

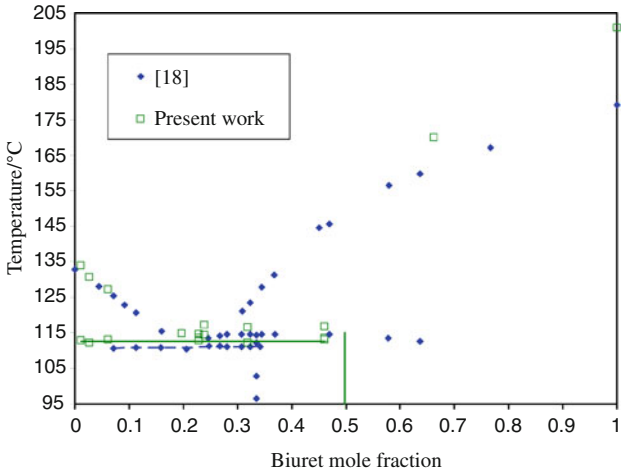

Fig. 6 Comparison of experimental results in the "urea–biuret" system (*diamonds* represent [18], *squares*—this study)

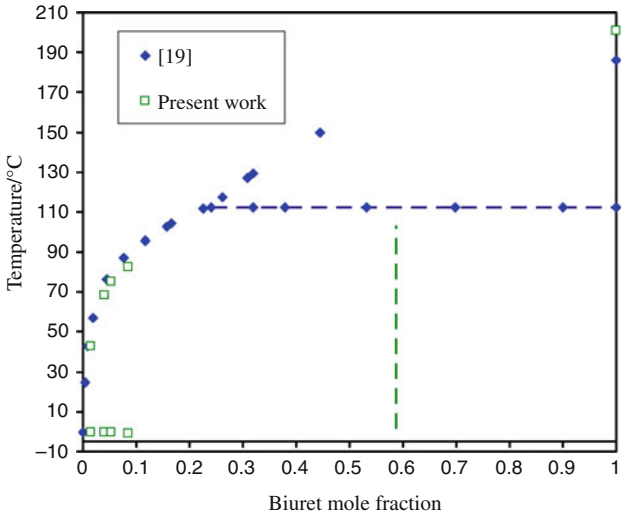

Fig. 7 Comparison of experimental results in the "water–biuret" system (*diamonds* represent [19], *squares*—this study)

evidence of the binary compound's synthesis of *another* composition (possibly of 50 mol% biuret). This suggestion does not conflict with the existing experimental data and correlates with the JCPDS information (the card #47-1948 corresponding with the compound $(NH_2)_2CO{\cdot}(NH_2CO)_2NH$). On the other hand, the powder X-ray diffraction databank has no card for the phase $2(NH_2)_2CO{\cdot}(NH_2CO)_2NH$ proposed in [18]. Unfortunately, our attempts to synthesize this compound in a single-phase form were unsuccessful.

Water–biuret system

Samples with biuret content varying from 1.4 to 8.5 mol% were prepared for studying liquidus and solidus. The solidus temperature was precisely reproduced during a thermal analysis of the water-rich mixtures. Liquidus peaks turned out unclear, taking us two or three attempts to define the exact effect temperature for every given composition.

Results of our study can be seen in Table 4. They are plotted on Fig. 7 along with the data from [19]. Figure 7 shows that these results confirm the coordinates of the incongruently melting biuret hydrate's liquidus.

Biuret hydrate $(NH_2CO)_2NH{\cdot}xH_2O$ appears in the "water–biuret" system. A lack of common opinion on its composition became the reason for us to choose its thermal stability and exact formula as the objective of our study.

According to the DSC results, the substance undergoes three transformation stages followed by heat effects. The first one (at 81 °C) is apparently the evaporation of absorbed water (not chemically bonded). The second one (at 111 °C) is the decomposition of crystal hydrate. Third is the biuret fusion and decomposition. Additional checks were conducted after 3, 10, and 13 days to make certain the hydrate was stable while in storage. For the entire period the substance visually had not changed: the hydrate remained a crispy white powder.

TG results proposed the $C_2N_3O_2H_5{\cdot}0.7H_2O$ formula for the biuret hydrate. Test measurements after 3 and 7 days confirmed the obtained value.

In order to identify the composition more precisely, the CHN analysis of the hydrate was performed two times. Biuret and water generate the crystal hydrate of the $C_2N_3O_2H_5{\cdot}(0.70 \pm 0.05)H_2O$ formula, based on mean values of the element content.

According to TG and elemental analysis, the biuret–water ratio in biuret hydrate equals 10:7.

Table 4 Liquidus and solidus coordinates for the "water–biuret" system according to DSC results

Biuret mole concentration/%	*t*/°C (solidus)	*t*/°C (liquidus)
1.4	−0.3	42.6
4.1	−0.5	68.6
5.2	−0.4	75.2
8.5	−0.7	83.5

Water–urea system

Eight mixtures with urea content ranging from 0.9 to 20.9 mol% were prepared for the study of liquidus and solidus. Obtained results are shown in Table 5.

Liquidus peaks are clear only if the urea concentration is low (up to 4.8 mol%).

Solidus and liquidus coordinates obtained in this study and published are plotted in Fig. 8. Our results reproduce the eutectic temperature and specify the area of the left liquidus curve ($T_{eut} = -12.3$ °C).

Table 5 Liquidus and solidus coordinates for the "water–urea" system according to DSC results

Urea mole concentration/%	*t*/°C (solidus)	*t*/°C (liquidus)
0.9	−12.0	−3.2
2.3	−12.1	−5.1
4.8	−11.8	−5.5
7.0	−12.0	–
12.1	−11.8	–
18.6	−12.2	–
19.6	−12.0	–
20.9	−12.0	–

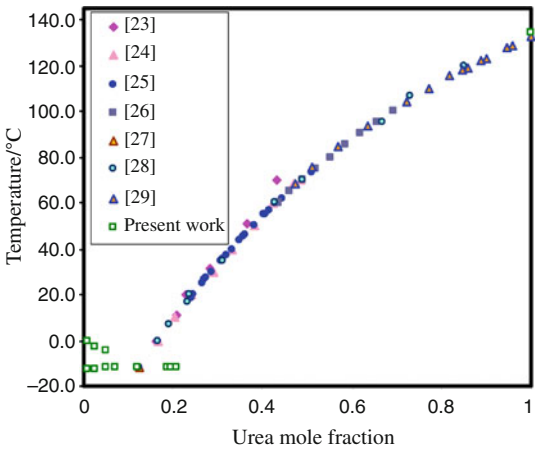

Fig. 8 Comparison of experimental results in the "water–urea" system (*squares* represent this study)

Conclusions

Decomposition and melting of biuret share the same temperature range. Estimation for biuret enthalpy of fusion and melting temperature was proposed. Recommended values are $\Delta_m H = (26.1 \pm 0.5)$ kJ mol^{-1}, $T_m = (473.8 \pm 0.4)$ K.

Parts of binary state diagrams were studied experimentally; solidus and liquidus coordinates were obtained. Compositions of binary compounds appeared to be 1:1 in the "urea–biuret" system and 7:10 in the "water–biuret" system.

Obtained data on phases and phase equilibria in binary subsystems can be used further for the ternary system modeling.

Acknowledgements The authors are grateful to A.V. Babkin for his help in sample purification, A.F. Asachenko for NMR measurements, A.V. Dunaev for coupled TG–FTIR. This study was supported by URALCHEM OJSC. This study was performed at the User Facilities Center of Lomonosov Moscow State University.

References

1. Kucheryavy VI, Lebedev VV. Sintez i primenenie karbamida. Leningrad: "Khimia"; 1970.
2. Ruehrwein RA, Huffman HM. Thermal data. The heat capacity, entropy and free energy of urea. J Am Chem Soc. 1946;68(9): 1759–61.
3. Kozyro AA, Danilovich SV, Krasulin AP. Teploemkost', entalpiya plavleniya i termodinamicheskie svoistva mocheviny. Zh Prikl Khim. 1986;59(7):1456–9.
4. Gambino M, Bros JP. Capacite calorifique de l'uree et de quelques melanges eutectiques a base d'uree entre 30 et 140 °C. Thermochim Acta. 1988;127:223–36.
5. Andersson O, Matsuo T, Suga H, Ferloni P. Low-temperature heat capacity of urea. Int J Thermophys. 1993;14(1):149–58.
6. Kabo GJ, Kozyro AA, Diky VV, Simirsky VV. Additivity of thermodynamic properties of organic compounds in crystalline state, heat capacities and enthalpies of phase transition of alkyl derivatives of urea in crystalline state. J Chem Eng Data. 1995; 40:371–93.
7. Ferloni P, Della Gatta G. Heat capacities of urea, N-methylurea, N-ethylurea, N-(n)propylurea, and N-(n)butylurea in the range 200 to 360 K. Thermochim Acta. 1995;266:203–12.
8. Schmidt VA, Becker F. Die Bildungswarme von Nitrocellulofen, Nitroglycerin und anderen widuigen Beltandteilen von Treibmitteln. Z Gesamte Schiess Sprengstoffwes. 1933;33:280–2.
9. Huffman HM. Thermal data. XII. The heats of combustion of urea and guanidine carbonate and their standard free energies of formation. J Am Chem Soc. 1940;62(5):1009–11.
10. Kabo GY, Miroshnichenko EA, Frenkel' ML, Kozyro AA, Simirskii VV. Termokhimiya alkylproizvodnyh karbamida. Izv Akad Nauk SSSR Ser Khim. 1990;4:750–5.
11. Lide DR. CRC handbook of chemistry and physics. 83th ed. CNR Press; 2002.
12. Langer HG, Brady TP. Thermal reactions by automated mass spectrometric thermal analysis. Thermochim Acta. 1973;5: 391–402.
13. Stradella L, Argentero M. A study of the thermal decomposition of urea, of related compounds and thiourea using DSC and TG-EGA. Thermochim Acta. 1993;219:315–23.
14. Chen JP, Isa K. Thermal decomposition of urea and urea derivatives by simultaneous TG/(DTA)/MS. J Mass Spectrom Soc Jpn. 1998;46(4):299–303.
15. Schaber PM, Colson J, Higgins S. Thermal decomposition (pyrolysis) of urea in an open reaction vessel. Thermochim Acta. 2004;424:131–42.
16. Siemion P. Solid state reactions of potato starch with urea and biuret. J Polym Environ. 2004;12(4):247–55.
17. Carp O. Considerations on the thermal decomposition of urea. Rev Roum Chem. 2001;46(7):735–40.
18. Rollet A-P, Cohen-Adad R, Hackspill ML. Action de la chaleur sur les mélanges durée et de biuret. CR Acad Sci IIc Chim. 1949;18:199–201.
19. Rollet A-P, Cohen-Adad R. Le systeme eau-biuret. CR Acad Sci II C. 1951;2214–16.
20. Ostrogovich G, Cipau R. Uber das verhalten des wasserfreinen biurets bei hohen drucken und uber sienen kristalldimorphismus. Tetrahedron. 1969;25:3123–9.
21. Aida K. Infra-red absorption spectra and structure of biuret-hydrogen peroxide complexes. J Inorg Nucl Chem. 1962;25(2): 165–70.
22. Toyozo U, Katsunosuke M, Yutaka S. Infrared spectra of biuret-hydrate and its deuterated compound. Bull Chem Soc Jpn. 1969; 42:1539–45.

23. Speyers CL. Solubilities of some carbon compounds and densities of their solutions. Am J Sci. 1902;IV(14):293–302.
24. Pinck LA, Kelly MA. The solubility of urea in water. J Am Chem Soc. 1925;47(8):2170–2.
25. Shnidman L, Sunier AA. The solubility of urea in water. J Phys Chem. 1932;36(4):1232–40.
26. Kakinuma H. Communication to the editor: the solubility of urea in water. J Phys Chem. 1941;45(6):1045–6.
27. Frejacques M. Les base theoriques de la synthese industrielle de l'uree (theoretical basis of the industrial synthesis of urea). Chim et Ind. 1948;60(1):22–35.
28. Jänecke E. Über das system: H_2O–CO_2–NH_3. Z Elektrochem. 1930;36(9):645–54.
29. Miller FW Jr, Dittmar HR. The solubility of urea in water the heat of fusion of urea. J Am Chem Soc. 1934;56(4):848–9.
30. Zordan TA, Hurkot DG, Peterson M, Hepler LG. Enthalpies and entropies of melting from differential scanning calorimetry and freezing point depressions: urea, methylurea, 1, 1-dimethylurea, 1, 3-dimethylurea, tetramethylurea, and thiourea. Thermochim Acta. 1972;5(1):21–4.
31. Vogel L, Schuberth H. Some physicochemical data of urea near the melting point. Chem Technol (Leipz). 1980;32:143–4.
32. Bros JP, Gambino M, Gaune-Escard M, Huu NT. Heat storage. Heats of fusion and heat capacity of urea-based mixtures. Calorim Anal Therm. 1983;14:92–5.
33. Ozawa T. Thermoanalytical investigation of latent heat thermal energy storage materials. Thermochim Acta. 1985;92:27–38.
34. Della Gatta G, Ferro D, Barone G, Piacente V. Vapour pressures and sublimation enthalpies of urea and some of its derivatives. J Chem Thermodyn. 1987;19(9):915–23.